Angewandte Chemie
Eine Zeitschrift der Gesellschaft Deutscher Chemiker

Supporting Information

Sulfurized Composite Interphase Enables a Highly Reversible Zn Anode

L. Wu, H. Yuan, Y. An, J. Sun, Y. Liu, H. Tang, W. Yang, L. Cui, J. Li, Q. An, Y.-W. Zhang, L. Xu*, L. Mai**

Supporting information

Sulfurized Composite Interphase Enables a Highly Reversible Zn Anode

Lu Wu,[+[a]] Hao Yuan,[+[b]] Yongkang An,[[a]] Jianguo Sun,[[c]] Yu Liu, [[a]] Han Tang,[[d]] Wei Yang,[[a]] Lianmeng Cui,[[a]] Jinghao Li,[[a]] Qinyou An,[[a]] Yong-Wei Zhang,[*[b]] Lin Xu,[*[a], [e]] Liqiang Mai[*[a], [e]]

[a] L.Wu, Y. An, Y. Liu, W. Yang, L. Cui, J. Li, Prof. Q. An, Prof. L. Xu, Prof. L. Mai
State Key Laboratory of Advanced Technology for Materials Synthesis and Processing, School of Materials Science and Engineering, Wuhan University of Technology
Wuhan, 430070, China
E-mail: linxu@whut.edu.cn
mlq518@whut.edu.cn
[b] Dr. H. Yuan, Prof. Y. Zhang
Institute of High Performance Computing (IHPC), Agency for Science, Technology and Research (A*STAR),
1 Fusionopolis Way, #16-16 Connexis, Singapore 138632, Singapore
E-mail: zhangyw@ihpc.a-star.edu.sg
[c] Dr. J. Sun
Department of Materials Science and Engineering, National University of Singapore, Singapore 117574, Singapore
[d] Dr. H. Tang
Hubei Provincial Key Laboratory of Green Materials for Light Industry, School of Materials and Chemical Engineering, Hubei University of
Technology, Wuhan 430068, China
[e] Prof. L. Xu, Prof. L. Mai
Hubei Longzhong Laboratory, Wuhan University of Technology (Xiangyang Demonstration Zone)
Xiangyang 441000, China
[+] These authors contributed equally to this work

1. Experimental

1.1 Electrolyte Preparation.

The 1M $ZnSO_4$ electrolyte was obtained by dissolving in $ZnSO_4 \cdot 7H_2O$ (purchased from Aladin, AR) in deionized water to obtain a transparent solution. The optimized electrolyte was prepared by adding 10 mmol of 5-Fluorouracil (purchased from Sigma-Aldrich, ≥99%) into 1M $ZnSO_4$, denoted as the 0.01F/ $ZnSO_4$ electrolyte.

1.2 Synthesis of Ammonium Vanadium Oxide ($NH_4V_4O_{10}$, NVO).

The NVO was prepared by a facile hydrothermal method. Firstly, 2 g V_2O_5 was added into the 10 ml ammonia solution (30%) under stirring, the solution turned yellow. Subsequently, 70 ml oxalic acid solution ($C_2H_2O_4$, 0.1 M) was added to the above mixed solution. After stirring for half an hour, hydrochloric acid (HCl, 37%) was adopted to adjust the pH to 3.0. Then the solution was heated at 190 °C for 5 h in 100 mL Teflon-lined stainless-steel autoclave. Following, the precipitate was washed with deionized water by centrifugation several times, and then dried at 60 °C oven 12 h in a vacuum drying oven to obtain the final product. The electrode materials were made by mixing NVO (70%), Ketjen black (20%), and polytetrafluoroethylene (PTFE) binder (10%). Then, the mixture was uniformly dispersed in isopropanol solvent and rolled repeatedly until forming a film, and then the film was vacuum-dried for 12 h and transferred to a titanium mesh for use (mass loading at 3-5 mg/cm^2).

1.3 Electrochemical Tests.

The CR2025-type cells were assembled in ambient air using glass fiber and two different electrolytes of Zn//Zn symmetrical cells, Zn//Cu asymmetrical cells and Zn//NVO full cells. The full cells were tested in the voltage range of 0.4-1.8 V (vs. Zn^{2+}/Zn). For pouch-type full cell, the above mixture was then rolled on Ti mesh and finally dried at 60 °C for 12 h. The Zn foil (0.1 mm) and cathode were cut into 3 cm * 3 cm. The mass loading on the cathode side is 3-5 mg cm^{-2}. The long-term galvanostatic cycling was measured in a LAND battery systems (LAND CT3002) instrument. For three electrode measurements, the linear sweep voltammetry (LSV), chronoamperograms (CAs) and tafel plots were obtained by employing the CHI 760E electrochemical workstation (CHI760E, Chenhua, China), AC impedance spectroscopy plots were tested using a BioLogic VMP3 multichannel electrochemical workstation and a platinum foil and an Ag/AgCl electrode and served as the counter and reference electrodes, respectively. The pure anode with ZnS in-situ SEI layer was obtained by disassembling the battery cycled in 0.01F/ $ZnSO_4$ electrolyte, the oxidation operation to convert sulfite anions into sulfate anions, then using the water to remove sulfate anions, reassemble the anode into symmetrical batteries for electrochemical characterization.

1.4 Calculation Methods.

All the first-principle calculations were performed using Vienna Ab initio Simulation Package (VASP) with the projector-augmented wave (PAW) approach.[1][1] The generalized gradient approximation (GGA) in the form of Perdew-Burke-Ernzerhof (PBE) function applied for exchange-correlation interaction and DFT-D3 was employed for empirical van der Waals interaction correction. [2] The convergence tolerances of energy and force were 10-5 eV

and 0.02 eV/Å, respectively. AIMD simulations were performed to check the stability of $ZnS@SO_3$ under the NVT ensemble and Nosé thermostat at 300 K. [3] The time step was set to 1 fs. The dehydration energy is defined as follows:

$$Ed = E[*Zn(H_2O)_{x-1}^{2+}] + E(H_2O) - E[*Zn(H_2O)_x^{2+}]$$

where $E[*Zn(H_2O)_{x-1}^{2+}]$ and $E[*Zn(H_2O)_x^{2+}]$ are the energies of adsorbed ion cluster with (x-1) and x water molecules, respectively. $E(H_2O)$ is the energy of a water molecule.

1.5 Materials Characterization.

The micromorphology of Zn anode metal and cathode materials was revealed via field emission scanning electron microscopy (FESEM, JSM-7100F, JEOL, Japan) and a super-large depth of field 3D microscopic system (VHX-600E, KEYENCE, Japan). The crystal of Zn depositions and cathodes were detected by X-ray diffractometer using Cu Ka radiation (XRD, Bruker D8 Advance Diffractometer). Combination with in-situ optical microscopy and electrochemical workstation to explore in-situ microscope images in real-time. The properties of the composition in Zn anode were evaluated by X-ray photoelectron spectroscopy (XPS, AXIS SUPRA+, Kratos, Japan) and time of flight-secondary ion mass spectrometer (TOF-SIMS, nano TOFIII, Ulvac-Phi, Japan), Raman (LabRAM HR Evolution&SmartSPM, HORIBA, Japan). The electrolyte intrinsic properties were characterized by Fourier transform infrared spectroscopy (FTIR, Nicolt iS50, Thermo Fisher, American) and liquid-state nuclear magnetic resonance (NMR, Bruker AVANCE III HD 500 MHz, D_2O). The contact angle between the Zn and electrolyte was measured by a contact angle goniometer (Model 260, Ramé Hart, USA).

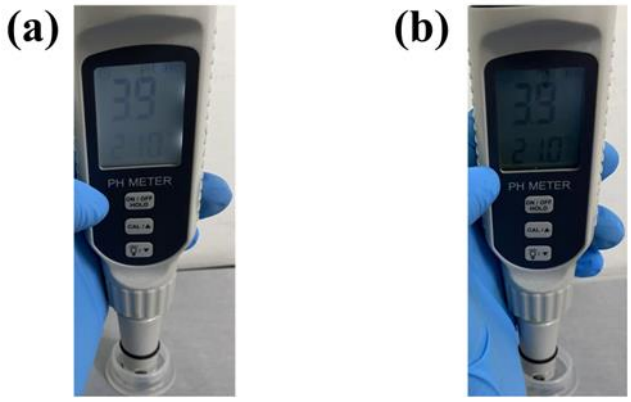

Figure S1. The pH of (a) 1M $ZnSO_4$ (b) Flu/$ZnSO_4$.

	1M $ZnSO_4$ (mS cm^{-1})	Flu/$ZnSO_4$ (mS cm^{-1})
Test 1	18.99	19.68
Test 2	18.82	19.12
Test 3	18.61	19.08
Ave	18.80	19.29

Figure S2. The ionic conductivity of 1M $ZnSO_4$ and Flu/$ZnSO_4$.

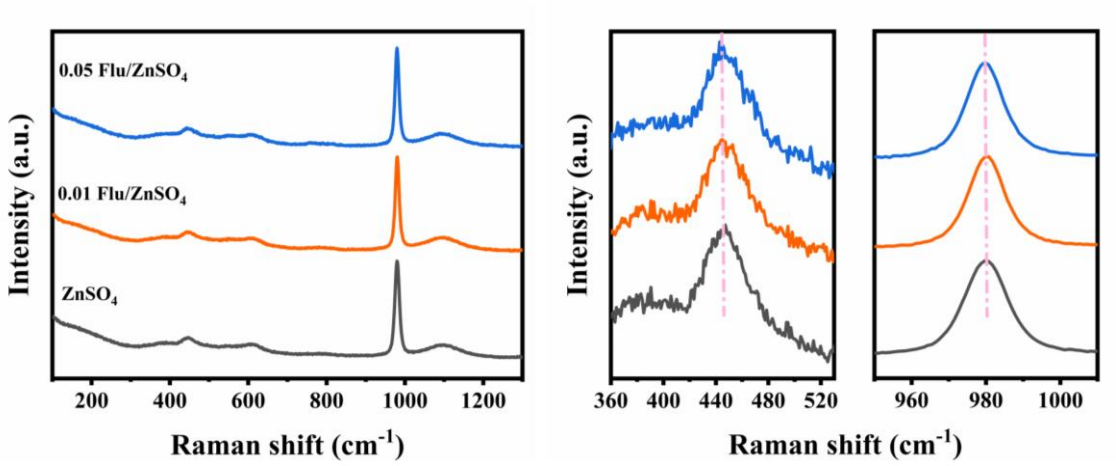

Figure S3. The Raman spectra for $ZnSO_4$, 0.01 M and 0.05 Flu/$ZnSO_4$ electrolyte.

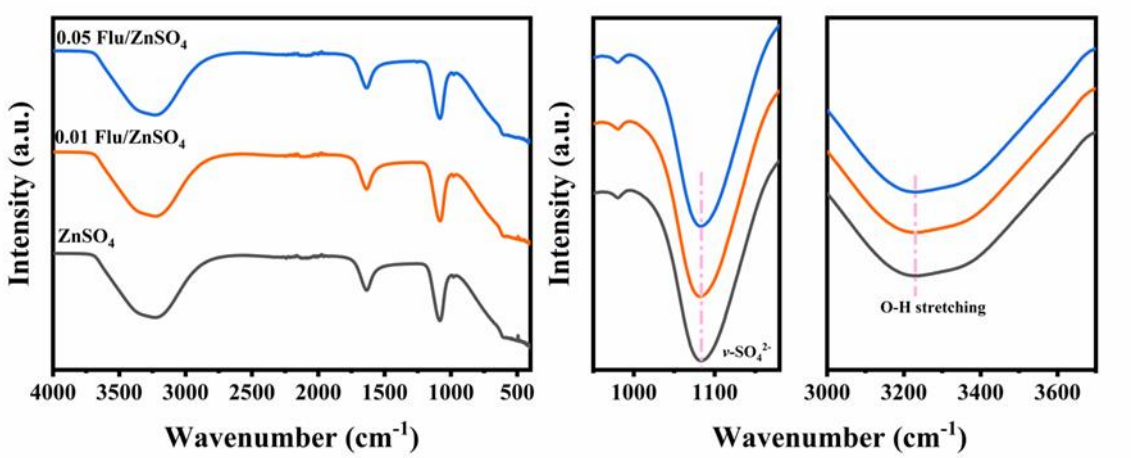

Figure S4. FTIR spectra for $ZnSO_4$, 0.01 M and 0.05 Flu/$ZnSO_4$ electrolyte.

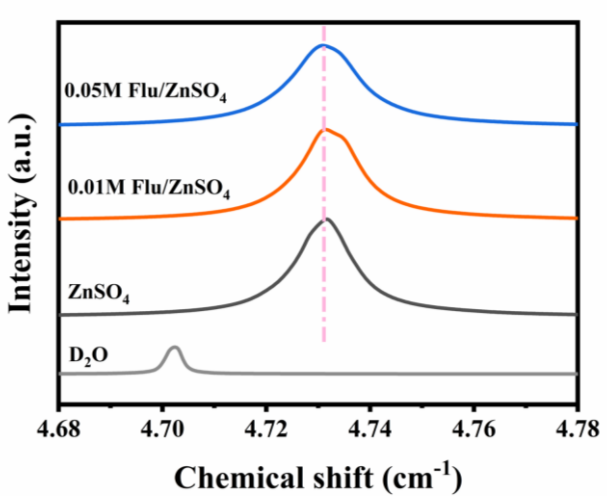

Figure S5. ^1H NMR spectra for $ZnSO_4$, 0.01 M and 0.05 M Flu/$ZnSO_4$ electrolyte.

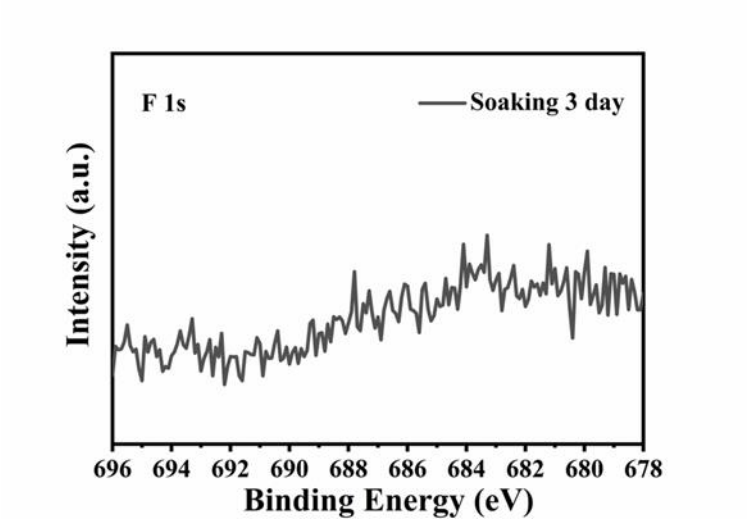

Figure S6. High-resolution XPS spectrum of F 1s of Zn anode soaked in Flu/$ZnSO_4$.

After the introduction of trace the 5-Flu additive, the pH of the electrolyte does not change, and the ionic conductivity has slightly increased from 18.8 to 19.29 mS cm^{-1} (Figures S1 and S2), indicating that the trace of the additive has a negligible effect on the physical properties of the electrolyte. The characterizations about solvation structures were measured by FT-IR, Raman and nuclear magnetic resonance (NMR). These results demonstrate that characteristic peak of the electrolyte with/without additives has no obvious peak shift (Figures S3, S4 and S5), indicating that the effect of Flu additive on the solvation structure is negligible. In addition, no signal of F was observed in the high-resolution F 1s spectrum of Zn foil soaked 3d in 0.01M Flu/$ZnSO_4$ (Figure S6), revealing that 5-Flu does not adsorb on the Zn anode surface to construct an electrolyte/electrode electric double layer.

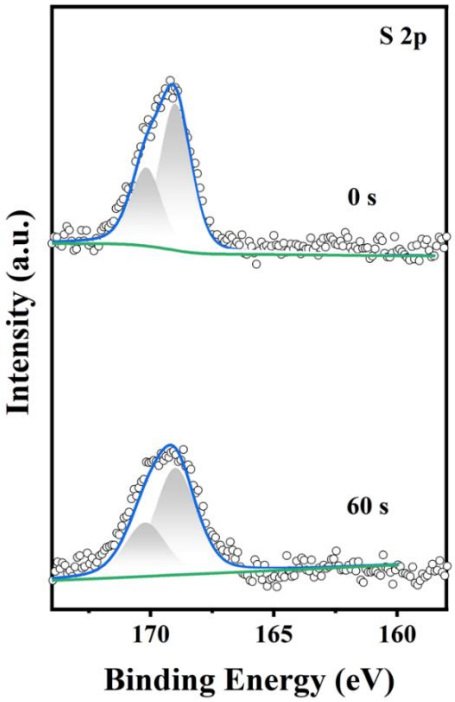

Figure S7. The XPS depth spectra of S 2p of Zn anode after 20 cycles with bare $ZnSO_4$ electrolyte.

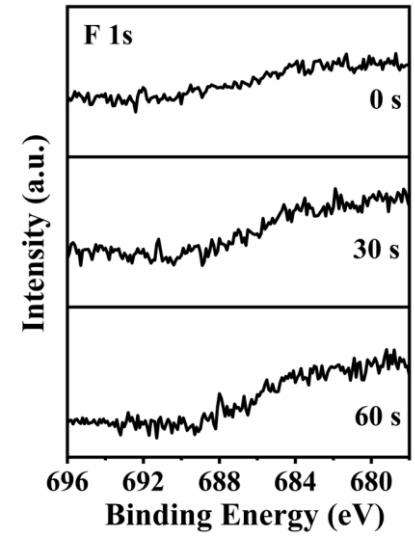

Figure S8. The XPS depth spectra of F 1s of Zn anode after 20 cycles with Flu/$ZnSO_4$ electrolyte.

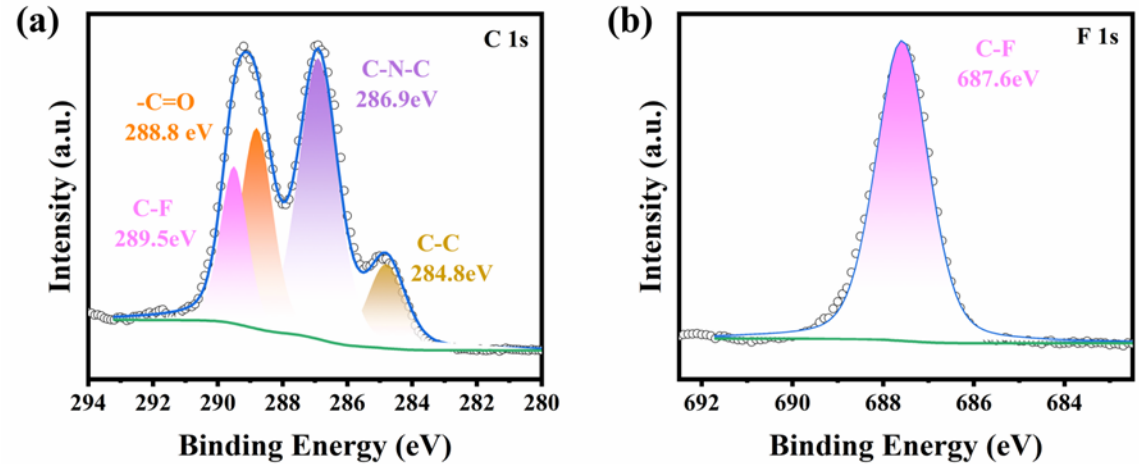

Figure S9. High-resolution XPS depth spectra of Flu powder of C 1s and F 1s.

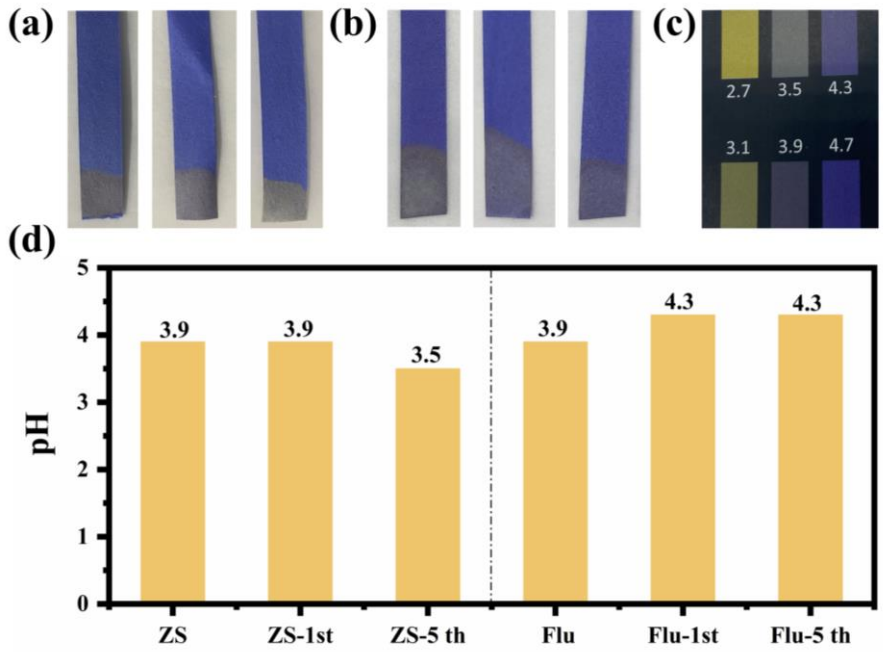

Figure S10. The pH evolution of Flu/$ZnSO_4$ during Zn plating/stripping. Images of the pH paper contacted with glass fibre separators. After initial soaking, after the first cycle and 5th cycles in (a) $ZnSO_4$ and (b) Flu/$ZnSO_4$ electrolyte. (c) Standard pH card. (d) pH changes as a function of cycle number at a current density of 1 mA cm^{-2} and areal capacity of 1 mAh cm^{-2}.

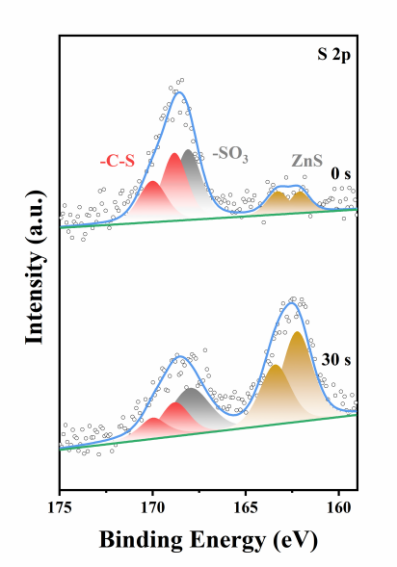

Figure S11. High-resolution XPS depth spectra of S 2p for Zn cycled in Flu/Zn(CF_3SO_3)$_2$ electrolyte. Ar^+ sputtering for 0s, 30s was conducted to generate depth profiles. Zn anode samples were obtained from Zn//Zn symmetric cells after 20 cycles of stripping/plating (1 mA cm^{-2}, 1 mAh cm^{-2}).

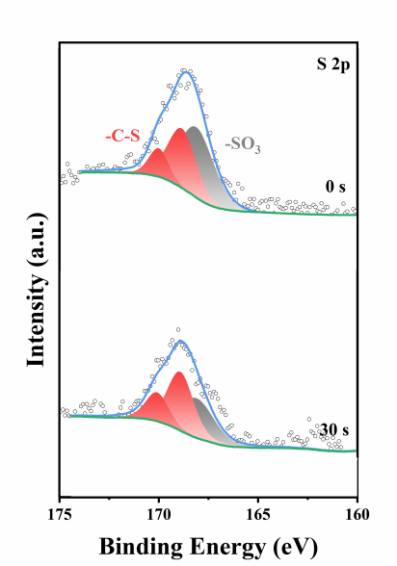

Figure S12. High-resolution XPS depth spectra of S 2p for Zn cycled in Zn(CF_3SO_3)$_2$ electrolyte. Ar^+ sputtering for 0s, 30s was conducted to generate depth profiles. Zn anode samples were obtained from Zn//Zn symmetric cells after 20 cycles of stripping/plating (1 mA cm^{-2}, 1 mAh cm^{-2}).

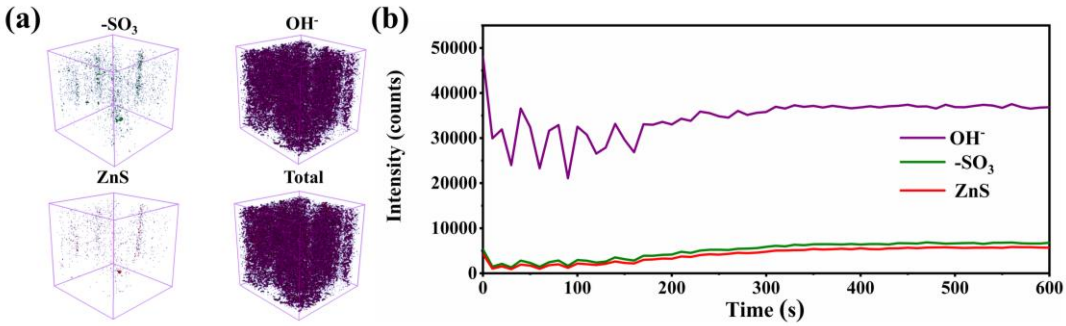

Figure S13. The TOF-SIMS 3D visualization of OH^-, $-SO_3$ and ZnS for the cycled Zn andoe in bare $ZnSO_4$ electrolyte.

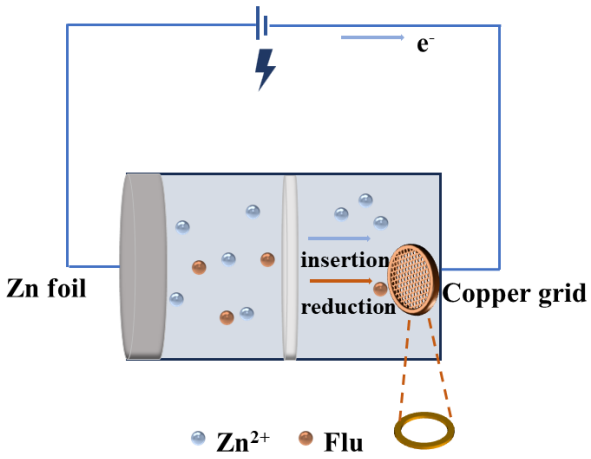

Figure S14. Schematic diagram of plated Zn on a copper grid forming the SEI layer at 4 mA cm^{-2} to prepare the TEM sample.

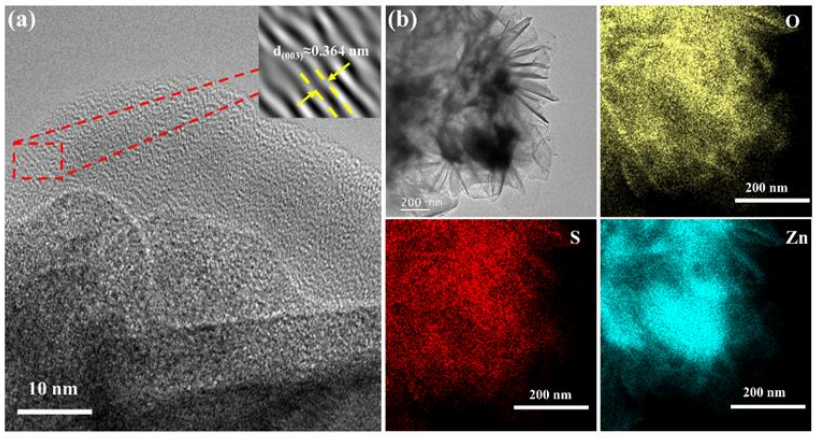

Figure S15. (a) HRTEM images and (b) HAADF image and corresponding elemental mapping of the sample of plated Zn on a copper grid cycled in $ZnSO_4$.

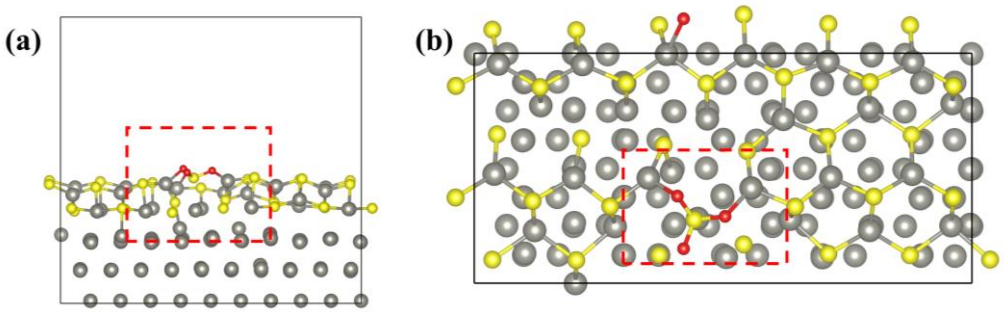

Figure S16. MD simulations of ZnS@SO_3 system of (a) elevation view and (b) vertical view of 3D snapshot in the initial stage.

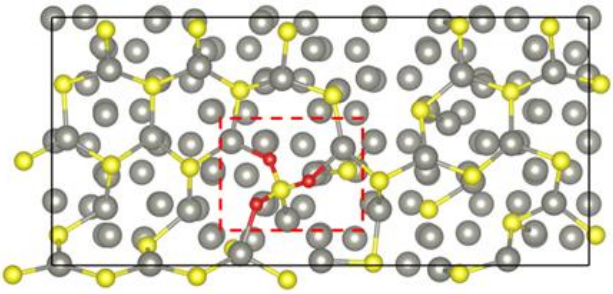

Figure S17. MD simulations of vertical view of 3D snapshot of the ZnS@SO_3 system at the time of 10 ps.

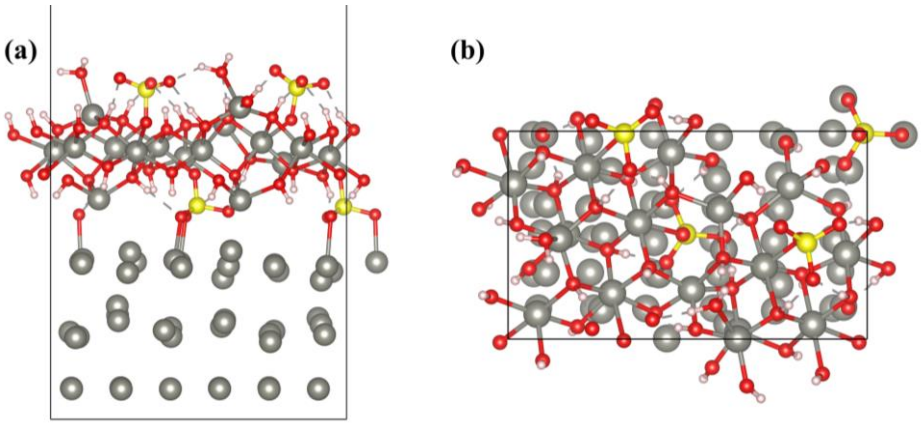

Figure S18. MD simulations of the ZSH@Zn system: (a) elevation view and (b) vertical view of the 3D snapshot in the initial stage.

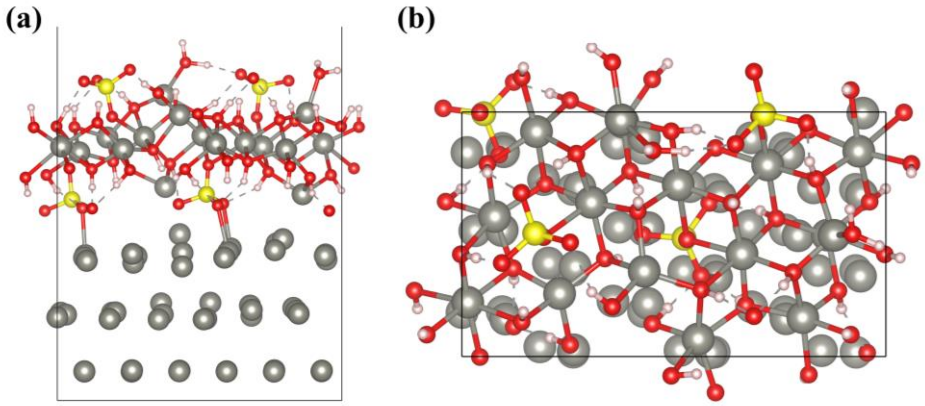

Figure S19. MD simulations of ZSH@Zn system: (a) elevation view and (b) vertical view of the 3D snapshot.at the time of 10 ps.

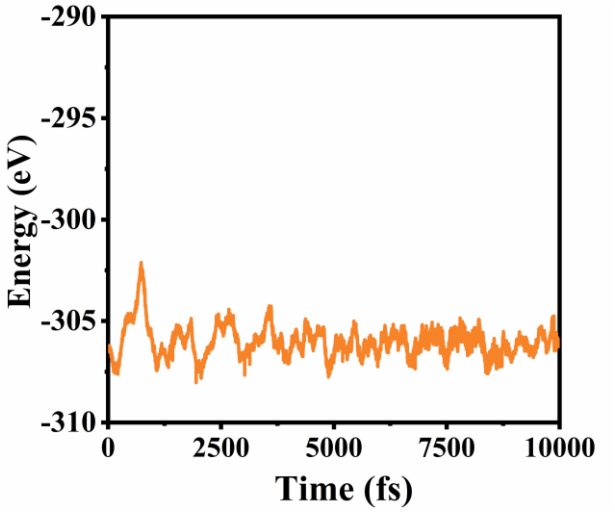

Figure S20. Time-dependent energy of ZSH@Zn system system.

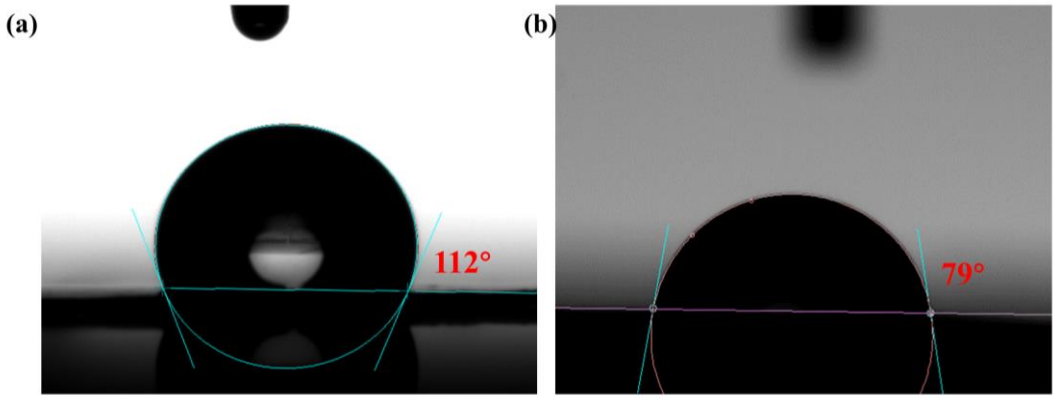

Figure S21. Contact angle measurement of an electrolyte droplet on (a)bare Zn and (b)SCSEI@Zn.

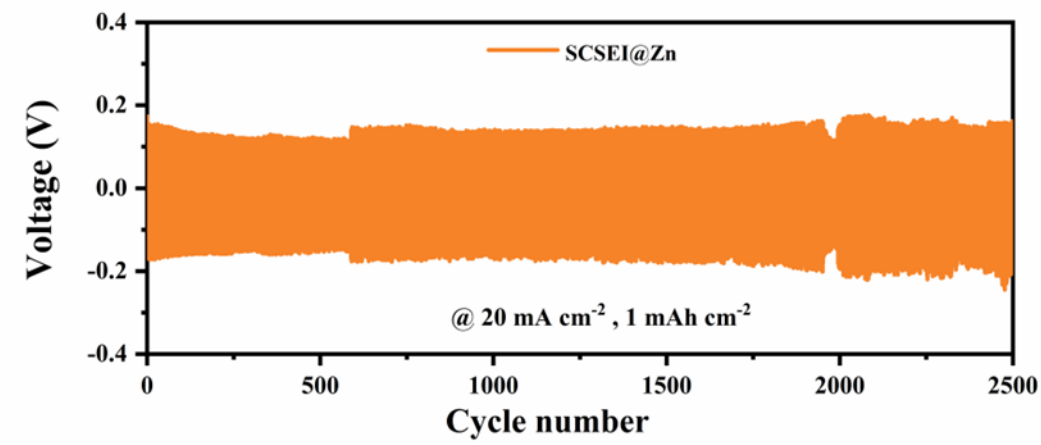

Figure S22. The cycling performance of Zn//Zn batteries at a current density of 20 mA cm^{-2}.

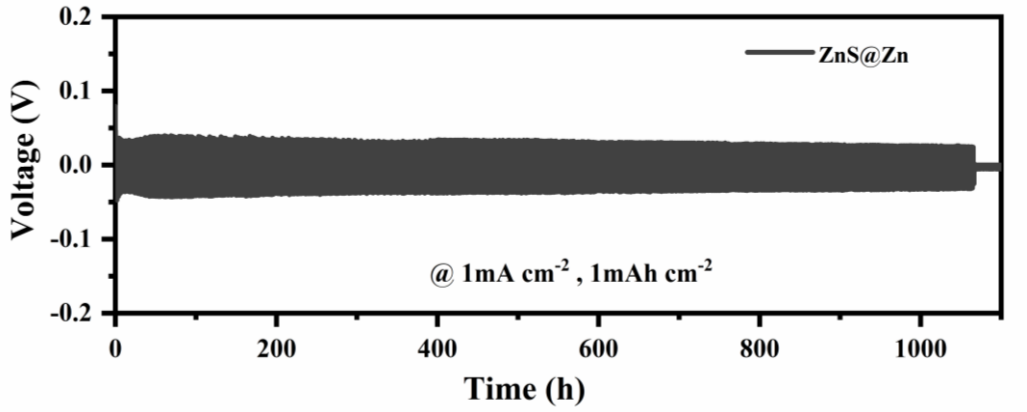

Figure S23. Cycling performance of symmetric Zn//Zn cells in ZnS@Zn at 1 mA cm $^{-2}$ with capacity of 1 mAh cm^{-2}.

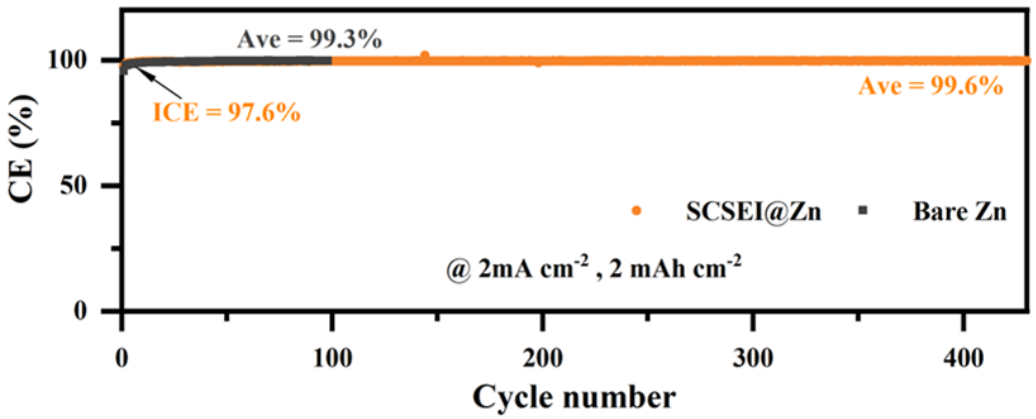

Figure S24. Coulombic efficiency of Zn // Cu cells using different electrolytes 2 mA cm^{-2} with capacity of 2 mAh cm^{-2}.

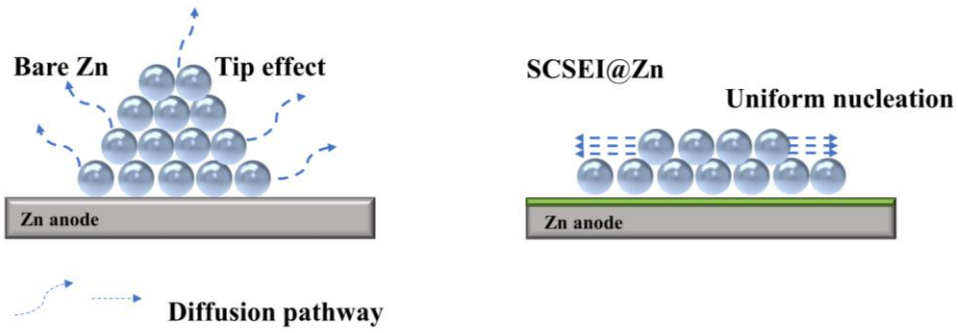

Figure S25. Schematic diagram of Zn^{2+} diffusion and nucleation on the Zn surface in two different electrolytes.Left panel: Bare Zn and right panel: SCSEI@Zn.

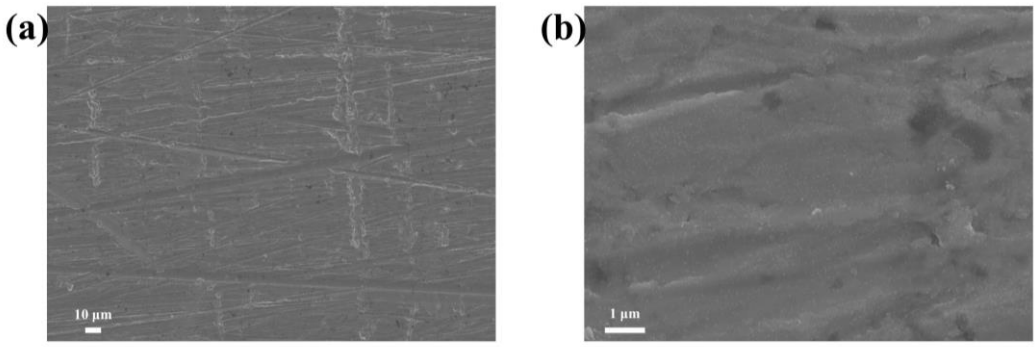

Figure S26. SEM images of bare Zn.

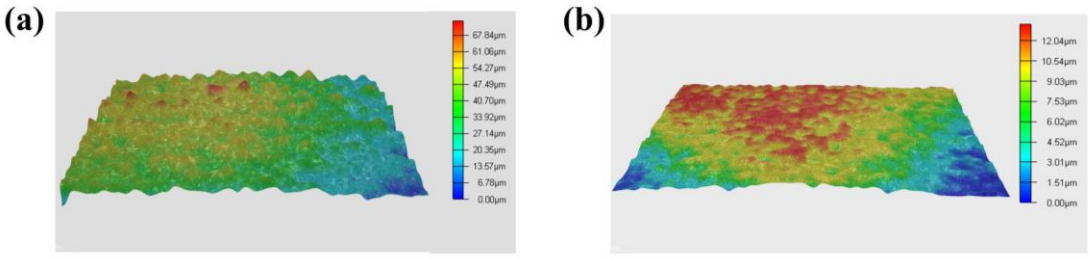

Figure S27. 3D confocal microscope image of different electrodes (a) Bare Zn and (b) SCSEI@Zn after 20 cycle tests at 1 mA cm^{-2} with a capacity of 1 mAh cm^{-2}.

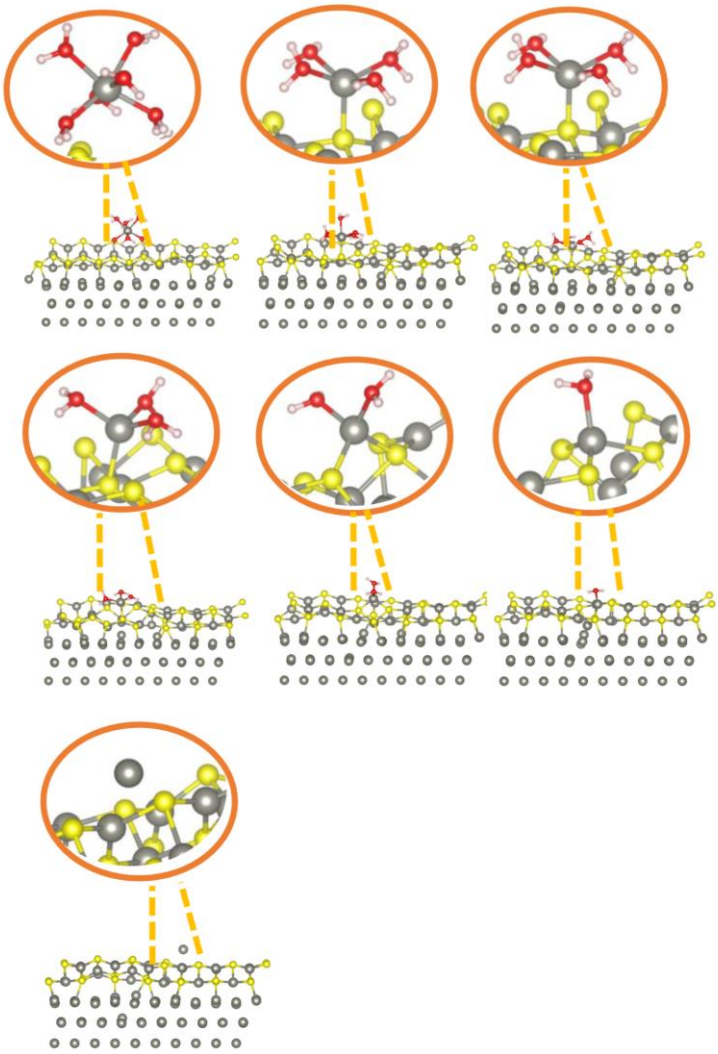

Figure S28. The migration process of Zn^{2+} with ZnS.

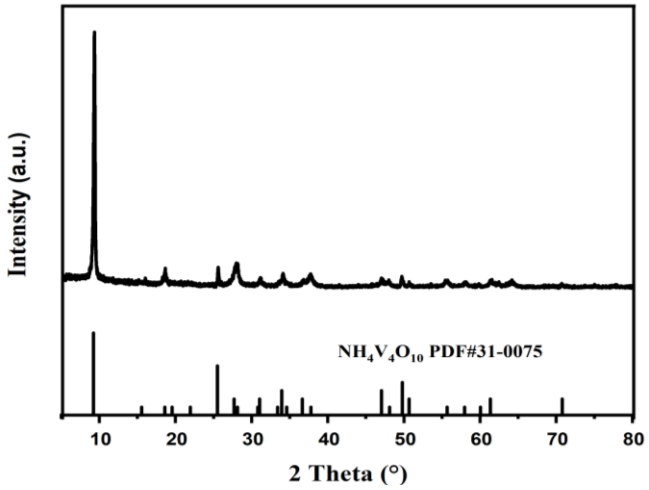

Figure S29. XRD pattern of NVO.

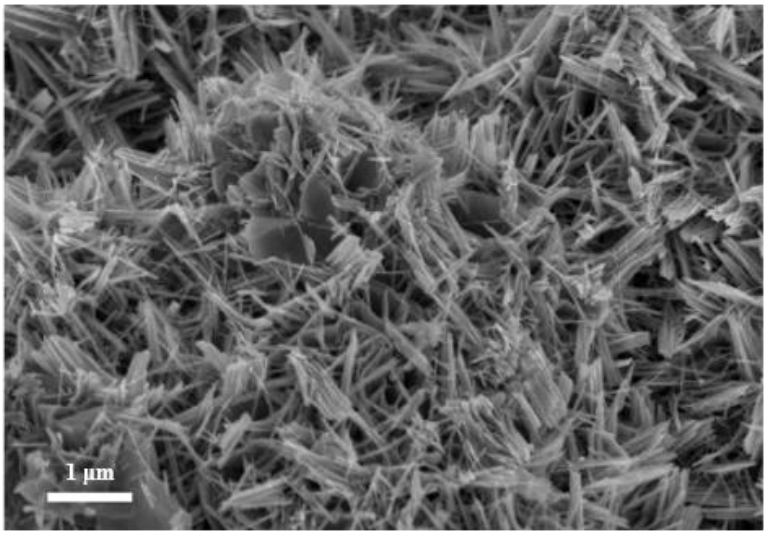

Figure S30. SEM image of NVO.

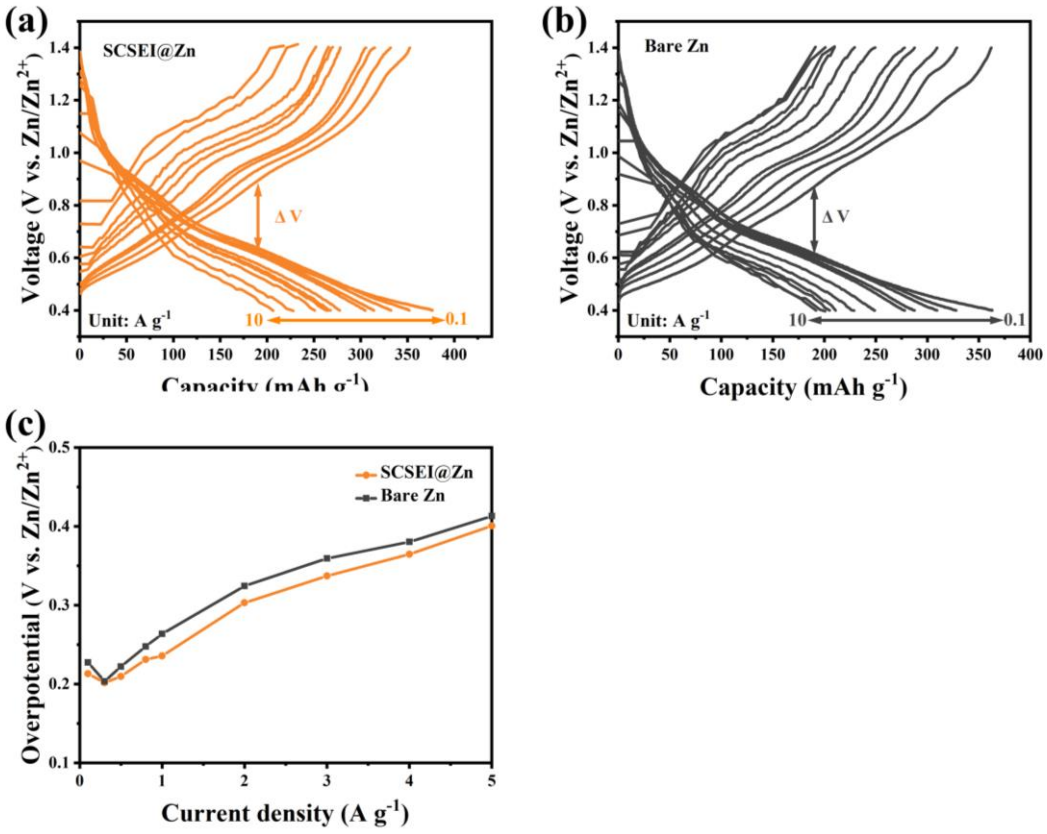

Figure S31.The corresponding discharge/charge profiles of the Zn//NVO coin cell at various current densities using (a) SCSEI, (b)bare Zn, and (c) comparison of the corresponding overpotential of the Zn//NVO full cells with SCSEI@Zn and bare Zn anodes.

Table S1. Summary of representative fluorochemicals additives modification strategies in zinc sulfate-based electrolyte

Additive and chemical formula	**Based electrolyte**	**Mechanism of action**	**Cycling lifespan in Zn//Zn cell (mA cm^{-22}, mAh cm^{-2})**	**Refs.**
10% TFA ($C_2H_2F_3NO$)	2M $ZnSO_4$	1. Break the H-bond network 2. Participation into solvation shell 3. Construct hybrid SEI of $Zn_4CO_3(OH)_6H_2O$ and ZnF_2	1500 (5.0, 1.0)	[4]
0.0025 mol SnF_2	1M $ZnSO_4$	1.Construct a synergistic fluoride/alloy composite artificial SEI layer 2. Simultaneously fill the voids between the Sn particles and Zn metal	1200 h (1.0, 1.0)	[5]
0.08M ZnF_2	2 M $ZnSO_4$	1. Regulate the growth orientation of zinc crystals 2. Serve as an inert protection layer against side reactions	600 h (1.0, 1.0)	[6]
1% vol FEC Fluoroethylene Carbonate ($C_3H_3FO_3$)	2 M $ZnSO_4$	1. Construct hybrid SEI of ZnF_2-riched inorganic/organic hybrid SEI (ZHS) layer 2. Regulate the solvated structure of Zn^{2+} to reduce H_2O	1000 h (4.0, 1.0)	[7]
3mM YTFPAA ($C_{24}H_{12}F_9O_6Y$)	2M $ZnSO_4$	1. Capture H^+ and thus buffer the decreased electrolyte pH 2. Preferred adsorption on zinc plane 3.Regulated by the dynamic electrostatic shielding effect of Y^{3+}	2100 h (0.5, 0.25)	[8]
0.05 M KPF_6	2 M $ZnSO_4$	1. Construct hybrid SEI of $Zn_3(PO_4)_2$ and ZnF_2 on the Zn anode	1200 h (2.0, 4.0)	[9]

Additiveand chemical formula	**Based electrolyte**	**Mechanism of action**	**Cycling lifespan in Zn//Zn cell (mA cm^{-2}, mAh cm^{-2})**	**Refs.**
8wt% Trifluoro ($C_6H_{13}ONBF_3$)	1 M $ZnSO_4$	1. Preferred adsorption on zinc plane 2. Construct favorable EDL	1800 h (1.0, 1.0)	[10]
5 mM TDFND ($C_9H_6F_{14}O_2$)	2 M $ZnSO_4$	1. Preferred adsorption on zinc (002) plane 2. Construct hybrid SEI of of ZnF_2	1200 h (1.0, 1.0)	[11]
0.1 g NH_4F	2 M $ZnSO_4$	1. Construct zinc fluoride (ZnF_2) layer with high Zn^{2+} conductivity	2500 h (1.0, 1.0)	[12]
[EMIm]TFSI ($C_8H_{11}F_6N_3O_4S_2$)	2 M $ZnSO_4$	1. Establish a water-scarce, Zn ion-rich HP system by in situ constructing a PEDOT:PSS hydrogel protective layer	1600 h (2.0, 1.0)	[13]
0.01M 5-Flu ($C_4H_3FN_2O_2$)	1 M $ZnSO_4$	Construct a -SO_3 and ZnS sulfide composite SEI (SCSEI) layer; -SO_3 can not only reduce the dehydration energy of $[Zn(H_2O)_6]^{2+}$, but also enhance the stability of the ZnS/Zn interface and homogenize the ZnS/Zn interface electric field, thereby significantly improving the dynamic kinetics and uniform deposition of Zn^{2+}.	2800 h (1.0, 1.0) 1500 h (10.0, 1.0)	This work

References

[1] a) G. Kresse, Phys. Rev. B 1996, 54, 11169-11186; b) G. Kresse, D. Joubert, Phys. Rev. B 1999, 59, 1758-1775.

[2] a) K. B. John P. Perdew, Matthias Ernzerhof, Phys. Rev. B 1996, 77, 3865-3868; b) S. Grimme, J. Antony, S. Ehrlich, H. Krieg, J. Chem. Phys. 2010, 132.

[3] S. Nosé, J. Chem. Phys. 1984, 81, 511-519.

[4] M. Wu, X. Wang, F. Zhang, Q. Xiang, Y. Li, J. Guo, Energy Environ. Sci. 2024, 17, 619-629. https://doi.org/10.1039/d3ee03040g.

[5] Y. Yang, G. Qu, Z. Wei, T. Hu, Y. Hu, Z. Wei, F. Mo, H. Li, G. Liang, Adv. Funct. Mater. 2024, 2409950. https:// doi: 10.1002/adfm.202409950.

[6] Y. An, Y. Tian, K. Zhang, Y. Liu, C. Liu, S. Xiong, J. Feng, Y. Qian, Adv. Funct. Mater. 2021, 31, 2101886. https://doi.org/10.1002/adfm.202101886.

[7] D. Xie, Y. Sang, D. H. Wang, W. Y. Diao, F. Y. Tao, C. Liu, J. W. Wang, H. Z. Sun, J. P. Zhang, X. L. Wu, Angew. Chem. Int. Ed. 2023, 62. https://doi.org/10.1002/anie.202216934.

[8] L. Li, C. Chen, P. Meng, Y. Zhang, Q. Liang, Adv. Funct. Mater. 2024, 2406965. https://doi.org/10.1002/adfm.202406965.

[9] Y. Chu, S. Zhang, S. Wu, Z. Hu, G. Cui, J. Luo, Energy Environ. Sci. 2021, 14, 3609-3620. https://doi.org/10.1039/d1ee00308a.

[10] Z. Zha, T. Sun, D. Li, T. Ma, W. Zhang, Z. Tao, Energy Storage Mater. 2024, 64, 103059. https://doi.org/10.1016/j.ensm.2023.103059

[11] T. Li, S. Hu, C. Wang, D. Wang, M. Xu, C. Chang, X. Xu, C. Han, Angew. Chem. Int. Ed. 2023, https://doi.org/10.1002/anie.2023.

[12] L. Ma, Q. Li, Y. Ying, F. Ma, S. Chen, Y. Li, H. Huang, C. Zhi, Adv. Mater. 2021, 33. 2007406. https://doi: 10.1002/adma.202007406.

[13] X. Huo, Z. Zhou, W. Huang, G. Gao, B. Li, J. Bi, Z. Du, W. Ai, Energy Environ. Sci. 2024. https:// doi: 10.1039/D4EE02909G.